ORIGINAL ARTICLE



Carboxymethyl cellulose grafted poly(acrylamide)/magnetic biochar as a novel nanocomposite hydrogel for efficient elimination of methylene blue

Seyed Jamaleddin Peighambardoust Down Mina Mollazadeh Azari Parisa Mohammadzadeh Pakdel Reza Mohammadi Reza Mohammadzadeh Reza

Received: 18 July 2024 / Revised: 10 September 2024 / Accepted: 18 September 2024 © The Author(s), under exclusive licence to Springer-Verlag GmbH Germany, part of Springer Nature 2024

Abstract

In the present study, the grafting of acrylamide (AAm) onto the carboxymethyl cellulose (CMC) backbone was performed using the free radical polymerization method to eliminate methylene blue (MB) from water media. Biochar (BC) was produced from tea waste by pyrolysis and doped with Fe3O4 nanoparticles. Magnetic biochar (MTWBC) nanoparticles were incorporated in CMC-g-P(AAm) hydrogel (HG) for the first time to enhance its adsorption properties. FTIR, XRD, TGA, VSM, BET, and SEM-EDS techniques characterized synthesized nanoparticles and adsorbents. The BET surface area for HG, HG/BC, and HG/MTWBC was obtained at 1.74, 2.011, and 3.58 m²/g, respectively, demonstrating how BC and MTWBC nanoparticles can enhance the surface area of HG. The magnetic saturation of MTWBC and HG/MTWBC was 15.45 and 1.85 emu/g, respectively. The maximum removal performance of HG, HG/BC, and HG/MTWBC nanocomposite hydrogels under optimum conditions of pH = 8, adsorbent dose 1.5 g/L, contact time 70 min, initial concentration 10 mg/L, and temperature 25 °C was obtained 83.22, 92.57, and 94.27%, respectively showing the effectiveness of BC and MTWBC nanoparticles in promoting removal performance of HG. Kinetic and equilibrium data followed Langmuir and pseudo-second-order models, respectively. The monolayer adsorption capacity for HG, HG/BC, and HG/MTWBC nanocomposite hydrogels was computed to be 12.3, 14.2, and 20.79 mg/g, respectively. The thermodynamic study showed that the MB elimination process is spontaneous and exothermic. The adsorption mechanisms of MB onto HG/MTWBC include hydrogen bonding, electrostatic interaction, and π - π interactions. Finally, it can be inferred that HG/MTWBC nanocomposite hydrogel can be applied as a novel, easy-separable, and efficient adsorbent to decontaminate MB from water media.

Keywords Carboxymethyl cellulose · Biochar · Magnetic Biochar · Nanocomposite hydrogel · Wastewater treatment

1 Introduction

One of the side effects of industrial development is the reduction of the quality of water sources. Yearly, industries' wastewater releases many pollutants into water bodies, affecting human health and organisms. Industries wastewater contains high levels of dyes, heavy metals, pesticides,

Seyed Jamaleddin Peighambardoust j.peighambardoust@tabrizu.ac.ir

Published online: 09 October 2024

and organic materials that enter the human body through the food chain. Methylene blue (MB) is an organic dye with a cationic nature widely applied in the leather, printing, paper, and textile industries. The excess amount of this dye in water resources leads to potentially harmful effects on human health, such as cyanosis, enhanced heartbeat rate, shock, tissue necrosis, vomiting, and jaundice, amongst others [1].

Researchers have always been looking for the best and most economical methods to remove pollutants from water sources, which have led to the development of the adsorption process, membrane filtration [2], oxidation [3], photocatalytic degradation [4], and coagulation [5] methods. Adsorption as an economical method without secondary pollution can be applied to solve this problem. Low cost, ease of operation, and simplicity of design are the main advantages of this method in comparison to other proposed ones [6].



Faculty of Chemical and Petroleum Engineering, University of Tabriz, Tabriz 5166616471, Iran

Polymer Research Laboratory, Department of Organic and Biochemistry, Faculty of Chemistry, University of Tabriz, Tabriz 5166616471, Iran

Hydrogels are three-dimensional, hydrophilic, and porous polymeric materials with wide applications in wastewater treatment, drug delivery, tissue engineering, and wound dressing. They can be applied as an efficient adsorbent with tunable properties in wastewater treatment applications. Due to low toxicity, low cost, and biodegradability, biopolymers such as Chitin [7], chitosan (CS) [8], carboxymethyl cellulose (CMC) [9], alginate (Alg) [10], and gelatin (GEL) [11] can be used to synthesis of hydrogels. For example, Algethami et al. extracted chitin from crab shells to synthesize chitin@metakaolin composite to decontaminate Cr(VI) ions. The single-layer adsorption capacity of the composite was found to be 278.88 mg/g [7]. Algarni et al. chitosan-Alginate@Fe/Mn mixed oxide nanocomposite to remove Cr(VI) ions. They showed that electrostatic interaction is the main mechanism of eliminating Cr(VI) ions [12]. Billah et al. prepared chitosan/Zn doped hydroxyapatite to remove methyl orange (MO) from water media. Also, they investigated the antibacterial activity of synthesized adsorbents towards Gram-positive and Gram-negative bacteria [13].

Also, abundant functional groups such as carboxyl and hydroxyl groups in these biopolymers' structures have made them promising candidates for preparing hydrogels as adsorbents. As a significant derivate of cellulose, CMC has been applied in diverse fields such as wastewater treatment, drug delivery, tissue engineering, and the food industry [14, 15]. This biopolymer is non-toxic, water-soluble, cheap, and pH-dependent due to the presence of a carboxyl group [6]. CMC-based hydrogels can react with cationic pollutants through electrostatic interaction and hydrogen bonding mechanisms.

The main drawbacks of biopolymers that need them to be treated by synthesized monomers such as itaconic acid (IA), acrylamide (AAm), acrylic acid (AA), and methacrylic acid (MAA), and their copolymer are low mechanical strength and adsorption capacity [16–18]. Besides using chemical methods such as grafting, embedding nanomaterials such as carbon-based materials, clays, metal oxides, and metal-organic frames (MOFs) is another way to solve this problem [19-22]. Carbon-based nanomaterials such as biochar, activated carbon, carbon nanotube, and graphene oxide (GO) have wide applications in wastewater treatment, sensors, electronics, catalysts, and energy storage. Biochar is a low-cost, biocompatible adsorbent with high porosity, surface area, and abundant functional groups. It is produced from the thermal decomposition of carbon-rich biomass substances such as lignocellulosic waste, municipal solid wastes, and sewage sludge in the absence of oxygen [23, 24].

Separating adsorbents from water media is one of the main issues that must be considered in adsorption. In conventional mode, adsorbents were separated from the water media using centrifuging, which is expensive and requires more energy. To solve this problem, the magnetic

separation method was developed and gained the attention of researchers in the last two decades [25]. This method allows magnetic adsorbents to be easily isolated from water media using a magnetic field [26]. Algethami et al. synthesized hydrochar-grafted chitosan to eliminate MG from water media. The results showed hydrochar-grafted chitosan removed 96.47% MG under optimum conditions [27].

Several studies applied clay and GO nanoparticles to wastewater treatment in HG. However, studies still need to be performed on using BC or magnetic BC as a lowcost nanomaterial in this hydrogel system. This work synthesized an innovative nanocomposite hydrogel to decontaminate MB from water media. Tea waste was used as a natural and abundant source to synthesize BC via pyrolysis and doped with magnetic nanoparticles (Fe₃O₄) by the chemical co-precipitation method. MTWBC was incorporated into CMC-g-P(AAm) hydrogel for the first time to elevate removal performance and ease separation from water media, which is performed by a magnetic field. The optimal adsorption process conditions were identified by assessing influencing variables in batch mode. More information on the mechanism of the adsorption process was obtained using kinetic, isotherm, and thermodynamic studies.

2 Materials and methods

2.1 Materials

CMC and potassium persulfate (KPS, 99.0%) were bought from Samchun, Korea. Acrylamide (AAm, 99.9%), methylene bisacrylamide (MBA, 99.0%), Iron (II) chloride tetrahydrate (FeCl₂·4H₂O, 99.9%), Iron (III) chloride hexahydrate (FeCl₃·6H₂O, 99.9%), sodium hydroxide (NaOH, 99.0%), methylene blue (MB, 99.0%) and hydrochloric acid (HCl, 38%) were purchased from MERCK, Germany. Tea was bought from a local shop, and deionized (DI) water was used throughout the experiments.

2.2 Biochar (BC) synthesis

First, the tea pulp was washed with hot water repeatedly until it lost color, and then it was dried in an oven at $100~^{\circ}\text{C}$ for 2 h. The dried tea pulp was placed in the furnace for 2 h at $500~^{\circ}\text{C}$ under an N_2 atmosphere to obtain BC. The obtained BC was powdered using the mill and meshed by sieves to ensure their size was lower than $125~\mu\text{m}$. Finally, the obtained biochar was stored in a container for further use.



2.3 Magnetic biochar (MTWBC) synthesis

MTWBC was prepared using the co-precipitation method. Firstly, $FeCl_2\cdot 4H_2O$ and $FeCl_3\cdot 6H_2O$ with a molar ratio of 1:2 were dissolved in 50 mL DI water, then 1 g of BC was added to it and stirred for 20 min. Then, 35 mL of NaOH with a concentration of 3 M was slowly mixed at 80–90 °C for 50 min. After the mentioned time, a magnet separated the magnetic composite from the aqueous solutions and washed it with water several times to make it completely neutral (pH=6–7). MTWBC was placed in an oven at a temperature of 90°C for 24 h to dry completely.

2.4 Synthesis of nanocomposite hydrogel

Firstly, a determined amount of CMC (0.33 g) was dissolved in hot DI water. A suspension solution of AAm (1.2 g), KPS (0.3 g), MBA (0.03 g), and MTWBC (10 wt. %) was prepared and sonicated for 30 min. The prepared suspension was added to the cold CMC solution and degassed for 5 min via N₂ gas. Then, the reaction bottle was put in the water bath at 65 °C. After 5 min, a gel was formed in the bottle and was kept in the water bath for 2 h to ensure complete polymerization. The prepared nanocomposite hydrogel was cut into small pieces and washed with DI water several times to remove unreacted components. Then, pieces of nanocomposite hydrogel were dried in a 60 °C oven for 24 h. The dried pieces were powdered using a mill and sieved via a 40-60 mesh sieve. Different nanocomposite hydrogel samples were prepared by varying the amount of MTWBC, and 10 wt.% was selected as the optimum value.

2.5 Characterization

The chemical structure of prepared samples was determined using FTIR spectroscopy (Tensor 27, Bruker, Germany) operating at a wavenumber of 400 to 4000 cm-1. X-ray diffraction (XRD) pattern of BC, MTWBC, HG, HG/BC, and HG/MTWBC adsorbents was recorded in an X-ray Diffractometer (Krisallofex D500, Siemens, Germany) equipped with Cu-K α ($\lambda = 1.54$ Å) radiation. The surface morphology of BC, MTWBC, HG, HG/BC, and HG/MTWBC adsorbents was analyzed by scanning electron microscopy (SEM, MIRA3, TESCAN, Brno, Czech Republic) operating at a voltage of 15 kV. Thermal study of prepared samples was determined using a thermogravimetric analyzer (TGA-PL, TGA 1500, Canada) operating at a heating rate of 10 °C/ min and temperature range of 25-900 °C under N₂ atmosphere. Specific surface area, mean pore diameter, and total pore volume of samples were calculated by gas sorption instrument (Asap 2020, Micro-metrics, USA).

2.6 Adsorption studies

The effect of adsorption parameters such as adsorbent dose (0.5--4~g/L), pH (2--10), initial concentration (10--50~mg/L), contact time (50--120~min), and temperature $(25\text{--}50~^\circ\text{C})$ on removal performance of BC, MTWBC, HG and HG/MTWBC adsorbents was studied to determine optimum condition. For this purpose, the pH of the MB solution was adjusted using 0.1 M HCl or NaOH solution, and 0.045 g of adsorbent was added to 30 mL of it and stirred at 500 rpm. After ending adsorption time, adsorbents were separated from the solution using a centrifuge and magnetic field. The concentration of remaining MB was determined using UV–Visible spectrophotometer (Shimazdu-1800, Japan) at $\lambda_{max} = 620~\text{nm}$. The removal percentage (R%) and equilibrium adsorption capacity (q_e) were calculated using the following equations:

$$R(\%) = \frac{MB_i - MB_t}{MB_i} \times 100 \tag{1}$$

$$q_e = \frac{(MB_i - MB_e)}{m}V \tag{2}$$

where MB_i (mg/L), MB_e (mg/L), V (mL), and m (g) are the initial and equilibrium MB concentration, volume of dye solution, and mass of adsorbent, respectively.

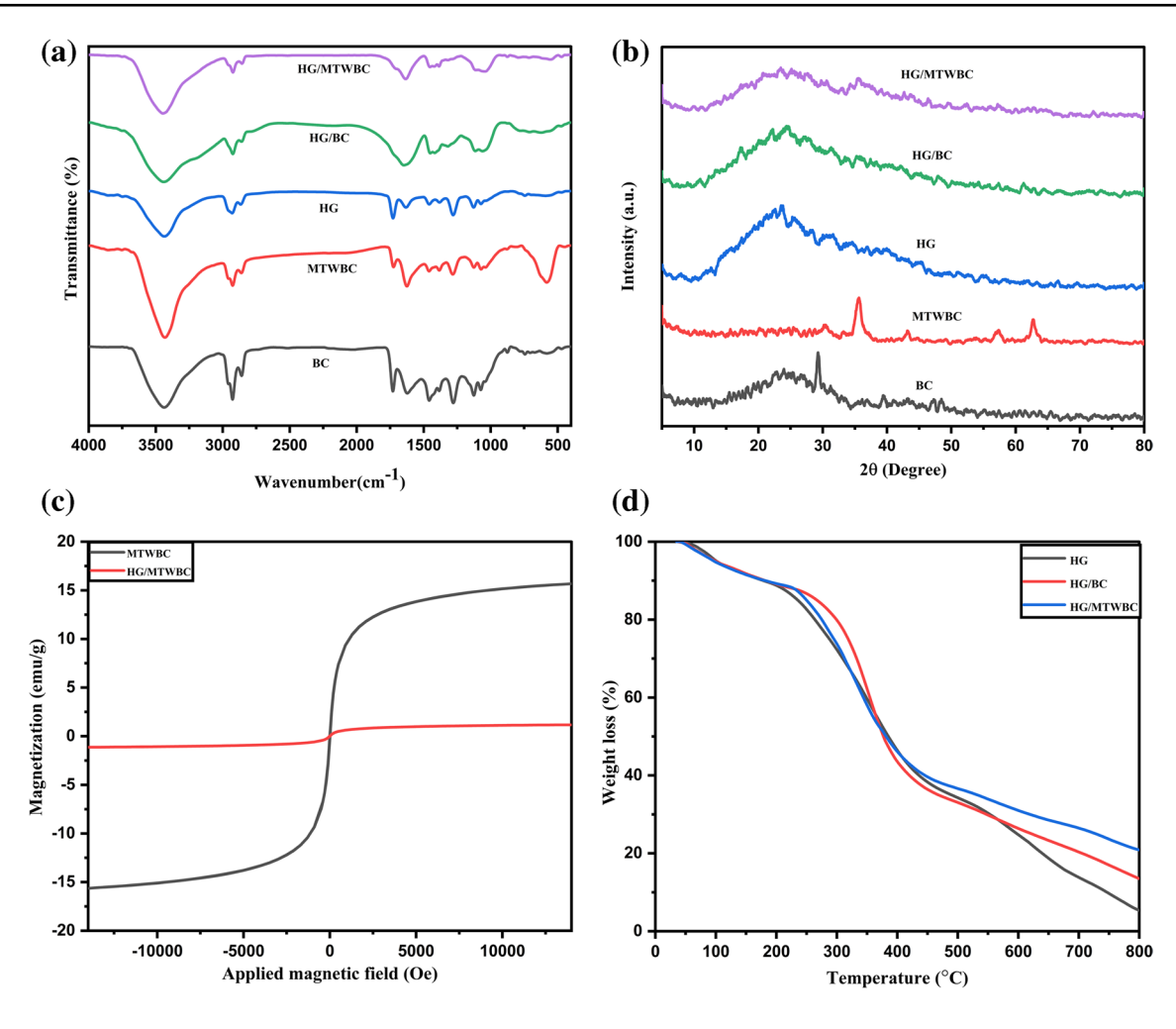
3 Results and discussion

3.1 Characterizations

The FTIR spectra of BC, MTWBC, HG, HG/BC, and HG/ MTWBC adsorbents before MB adsorption were depicted in Fig. 1a. In the FTIR spectra of BC, 3437, 2996, 1725, 1625, and 1073 cm⁻¹ peaks, can be assigned to stretching vibrations of -OH, -CH, -C = O, C = C, and -C-O, respectively. FTIR spectra of MTWBC show that the intensity of some BC peaks was changed after integrating Fe₃O₄, showing good interaction of these nanoparticles with BC. Also, the observed sharp peak at 581 cm⁻¹ can be related to the -Fe-O bond, which confirms the successful formation of Fe₃O₄ nanoparticles on BC [28]. In the spectra HG, HG/ BC, HG/MTWBC adsorbents nanocomposite hydrogel, peaks of -OH and -NH groups were overlapped around a wavenumber of 3500 cm⁻¹ and also observed peaks around 1729, 1624, 1280, and 1072 cm⁻¹ corresponded to stretching vibrations of -C = O, -N-H, -C-O, and -C-O-C bonds, respectively.

XRD pattern of BC, MTWBC, HG, HG/BC, and HG/MTWBC adsorbents was depicted in Fig. 1b. In the XRD





 $\mbox{Fig. 1 \ a) FTIR analysis, b) XRD patterns, c) VSM, d) TGA, and e-g) BET of BC, MTWBC, HG, HG/BC, and HG/MTWBC nanocomposite hydrogel \\$

pattern of BC, the observed wide peak centered at 25° can be related to the crystal plane index C(002) [29]. In the XRD pattern of MTWBC, characteristic peaks of Fe₃O₄ nanoparticles located at 35.8, 43.5, 57.8, and 64° were observed, showing the presence of these nanoparticles on BC [30]. Also, it shows that the crystalline structure of Fe₃O₄ nanoparticles is preserved after integration with BC [31]. In the XRD pattern of HG, HG/BC, and HG/MTWBC adsorbents, a wide broad peak was observed at 20.5°, showing an amorphous structure.

VSM analysis was applied to assess the magnetic properties of MTWBC and HG/MTWBC nanocomposite hydrogel at room temperature. As demonstrated in Fig. 1c, the magnetic saturation of MTWBC and HG/MTWBC nanocomposite hydrogel is 15.45 and 1.85 emu/g, respectively. The decrease in the magnetic value of HG/MTWBC compared to MTWBC can be related to the low concentration of Fe₃O₄ nanoparticles in nanocomposite hydrogel [25].

The thermal stability of HG, HG/BC, and HG/MTWBC adsorbents was investigated by TGA analysis in the 25-800 °C temperature range. As demonstrated in Fig. 1d, the weight loss of samples happened in three stages. In the first stage, decomposition and the weight loss of HG, HG/BC, and HG/MTWBC adsorbents occurred in the temperature range of 45–263, 45–267, and 45- 268 °C, respectively and related to loss of moisture. The second weight loss can be ascribed to dehydration of the saccharide ring and happened in the temperature range of 263–501 °C, 267–503 °C, and 268-504 °C for HG, HG/BC, and HG/MTWBC adsorbents, respectively. The third stage of significant weight loss occurs in the temperature range of 501-800, 503-800, and 504-800 °C for HG, HG/BC, and HG/MTWBC adsorbents, respectively. In the third stage, polymer chains and crosslinked network destruction occur [21]. The total weight loss for HG, HG/BC, and HG/MTWBC adsorbents was found to be 94.98, 86.9, and 79.34%, respectively, showing the effectiveness of BC and MTWBC nanoparticles in promoting



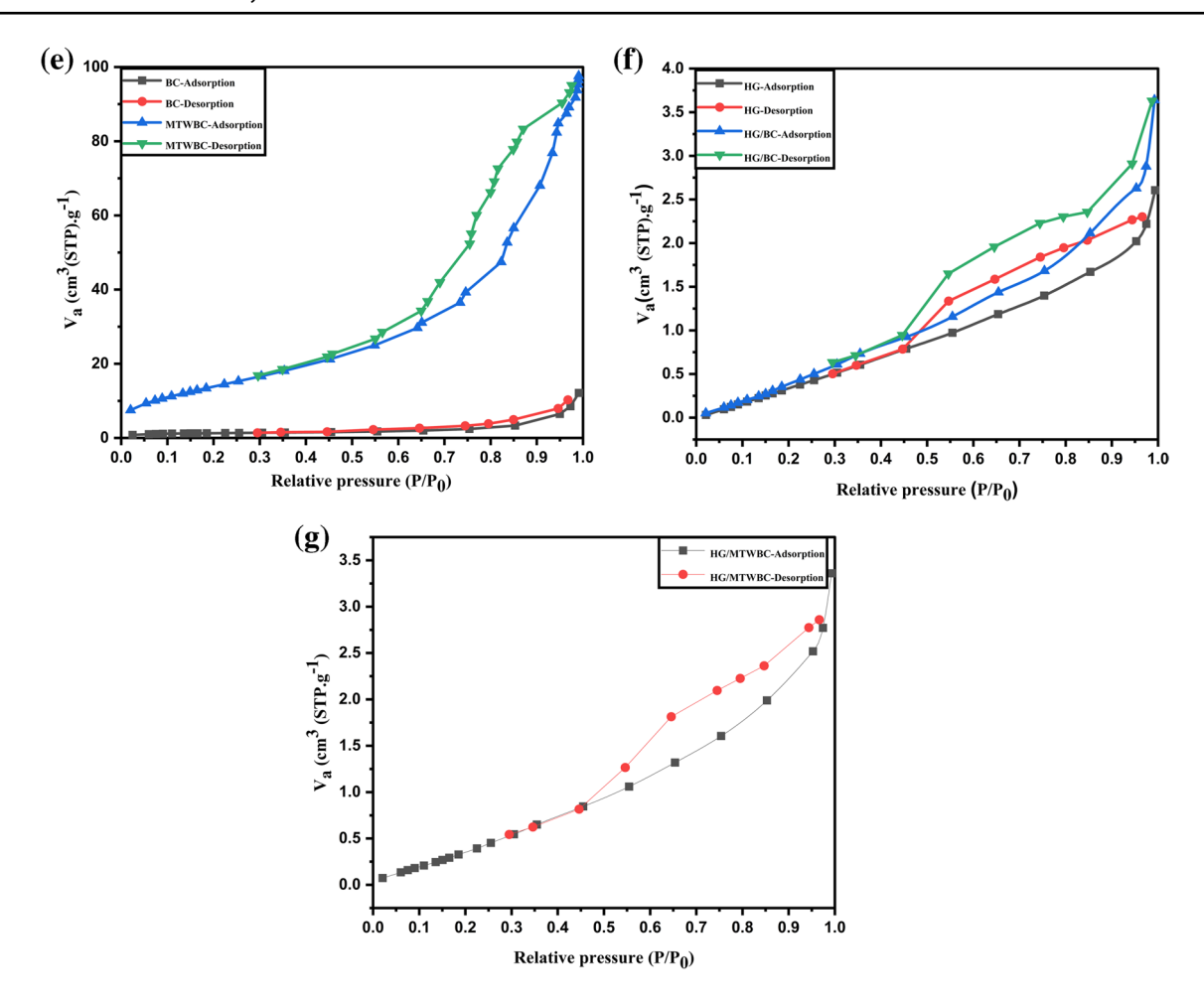


Fig. 1 (continued)

the thermal stability of hydrogel. These nanoparticles act as thermal barriers and limit heat diffusion to hydrogel structure.

To investigate the textural properties of BC, MTWBC, HG, HG/BC, and HG/MTWBC adsorbents, BET analysis was performed at a temperature of 77 K. The isotherm curves of N₂ ad(de)sorption for BC, MTWBC, HG, HG/BC, and HG/MTWBC adsorbents were depicted in Fig. 1eg. According to the IUPAC classification, the isotherm curves for MTWBC, HG, HG/BC, and HG/MTWBC adsorbents are type V, while BC is type IV [32]. The

textural properties of BC, MTWBC, HG, HG/BC, and HG/MTWBC adsorbents, such as surface area, total pore volume, and mean pore diameter, were tabulated in Table 1. The results showed that modification of BC with Fe₃O₄ nanoparticles significantly enhances the surface area and total pore volume. Also, adding BC and MTWBC to HG promotes surface area, so higher removal performance was expected from nanocomposite hydrogels than neat hydrogels. The mean pore diameter of all samples is 2–50 nm, so they are classified as mesopore materials.

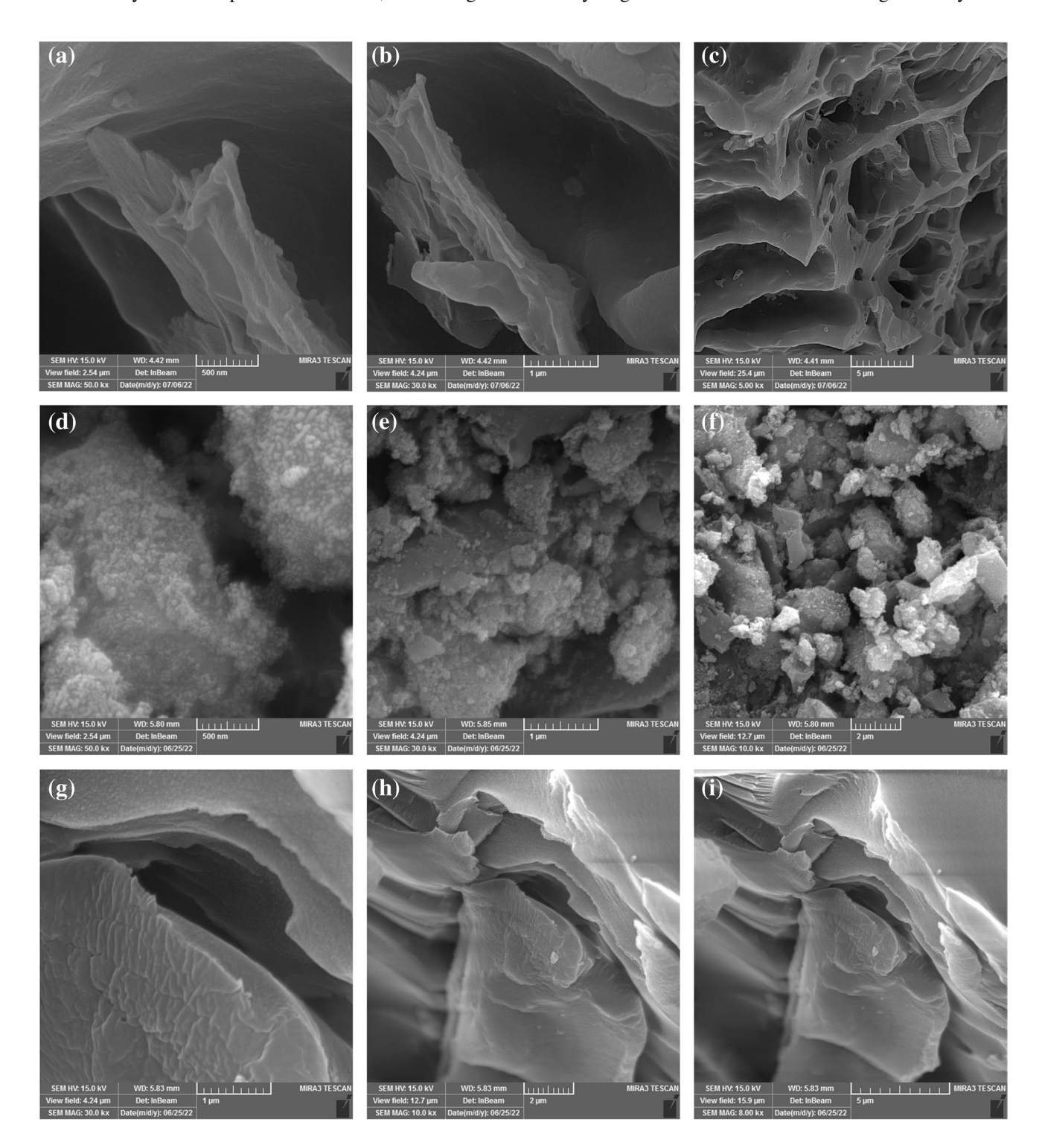
Table 1 Textural properties of BC, MTWBC, HG, HG/BC, and HG/MTWBC

Parameters		Adsorbent			
	BC	MTWBC	HG	HG/BC	HG/MTWBC
BET area (m ² /g)	4.53	51.92	1.74	2.011	3.58
Total pore volume (cm ³ /g)	1.042	11.92	0.4	0.46	0.48
Mean pore size (nm)	16.24	11.51	12.54	10.06	4.36



SEM-EDS analysis assessed the morphology of BC, MTWBC, HG, HG/BC, and HG/MTWBC adsorbents before and after MB sorption. As depicted in Fig. 2a-c, biochar has an irregular surface. The morphology of BC was changed after modification with Fe₃O₄ nanoparticles in such a way that some pores were formed, facilitating the

diffusion of MB molecules to interact with internal adsorption sites. Small spherical particles confirm the successful formation of Fe₃O₄ nanoparticles on the BC surface (Fig. 2df). A comparison of hydrogel and nanocomposite hydrogel morphology showed that the roughness and porosity of the hydrogel's surface were enhanced significantly after



 $\textbf{Fig. 2} \quad \text{FESEM images of } \textbf{a-c}) \; \text{BC}, \\ \textbf{d-f}) \; \text{MTWBC}, \\ \textbf{g-i}) \; \text{HG}, \\ \textbf{j-l}) \; \text{HG/BC}, \\ \text{and } \textbf{m-o}) \; \text{HG/MTWBC} \; \\ \text{with different magnification} \; \text{MTWBC}, \\ \textbf{g-i}) \; \text{HG/BC}, \\ \textbf{d-f}) \; \text{HG/BC}, \\ \textbf{$



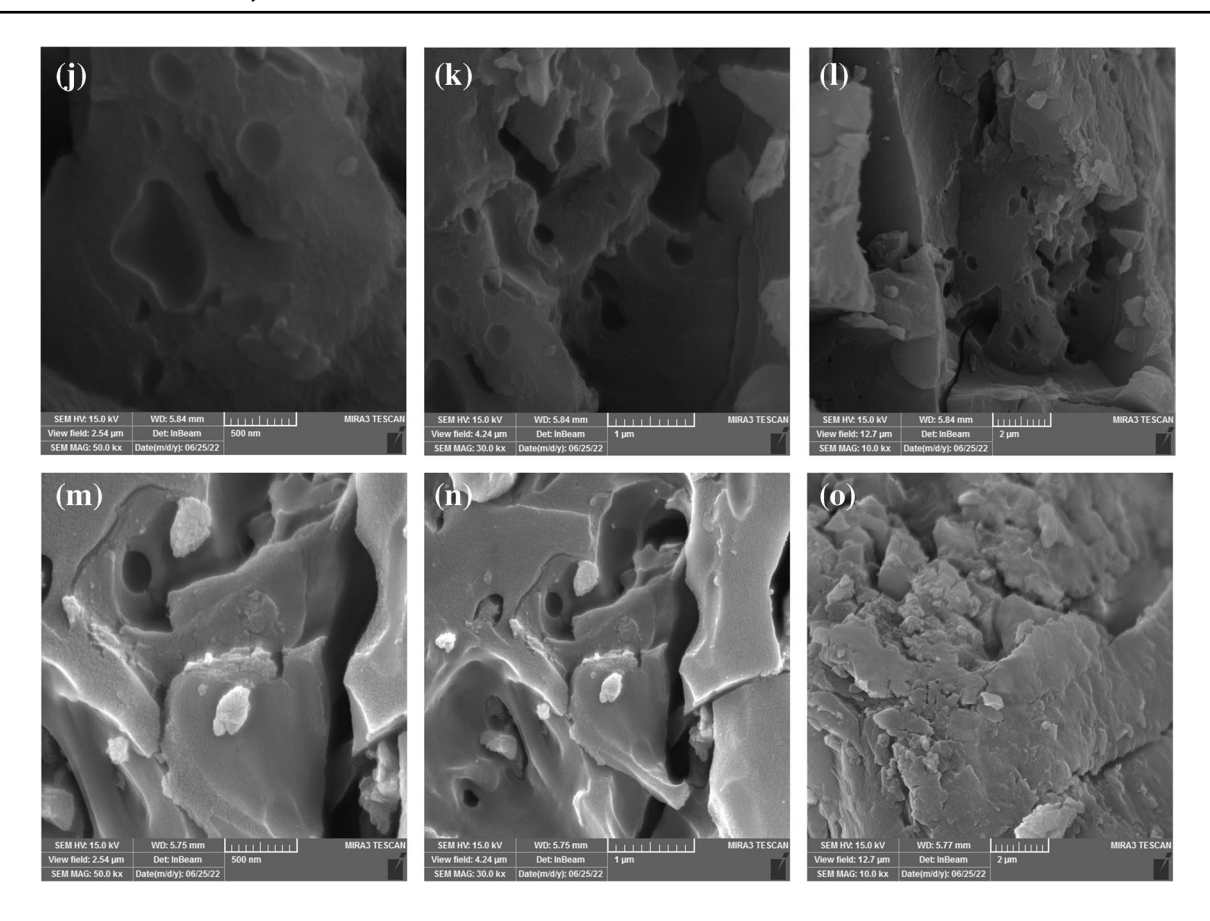


Fig. 2 (continued)

embedding BC and MTWBC nanoparticles (Fig. 2g-o). The chemical composition of BC, MTWBC, HG, HG/BC, and HG/MTWBC adsorbents was assessed by analysis. As demonstrated in Fig. 3a-d, the EDS spectra of samples showed the presence of C (74.8%) and O (25.2%) elements in BC, C (32%), O (33.63%), and Fe (34.37%) elements in MTWBC, C (42.69%), O (34.89%), and N (22.41%) elements in HG, C (49.67%), O (31.48%), and N (18.06%) elements in HG/BC, and C (29.96%), O (22.26%), Fe (15.745%), and N (6.62%) elements in HG/MTWBC nanocomposite hydrogel. Investigation of the morphology of BC, MTWBC, HG, HG/BC, and HG/MTWBC adsorbents after MB adsorption showed that the surface of adsorbents gets smoother and most of the pores were filled by MB molecules (Fig. 4a-e).

3.2 Investigation of sorption parameters on elimination of MB

3.2.1 Impact of ph

Due to abundant ionizable functional groups in the synthesized adsorbents' structure, their removal performance depends highly on pH. The impact of pH on the removal performance of BC, MTWBC, HG, HG/BC, and HG/

MTWBC adsorbents was investigated at an adsorbent dose of 1.5 g/L, contact time of 70 min, initial concentration of 10 mg/L, and temperature of 25 °C. As presented in Fig. 5a, the removal performance of BC, MTWBC, HG, HG/BC, and HG/MTWBC adsorbents was enhanced from 33.27 to 90.15%, 38.79 to 95.58%, 31.85 to 83.22%, 34.26 to 92.57%, and 36.23 to 94.27%, respectively. In an acidic medium, the low removal performance of synthesized adsorbents can be related to the competition of H⁺ ions and MB molecules to sorption to active sites. The size of H⁺ ions is smaller than that of MB⁺ molecules, so they can diffuse more easily into the adsorbent structure and interact with adsorption sites. By elevating pH, carboxyl groups of adsorbents were ionized, so the removal performance was enhanced, and most parts of MB molecules were adsorbed through electrostatic interactions [33]. An optimum pH of 8 was selected for further adsorption experiments.

3.2.2 Impact of adsorbent dose

The impact of adsorbent dose on the removal performance of BC, MTWBC, HG, HG/BC, and HG/MTWBC adsorbents was assessed in the range of 0.5 to 4 g/L.



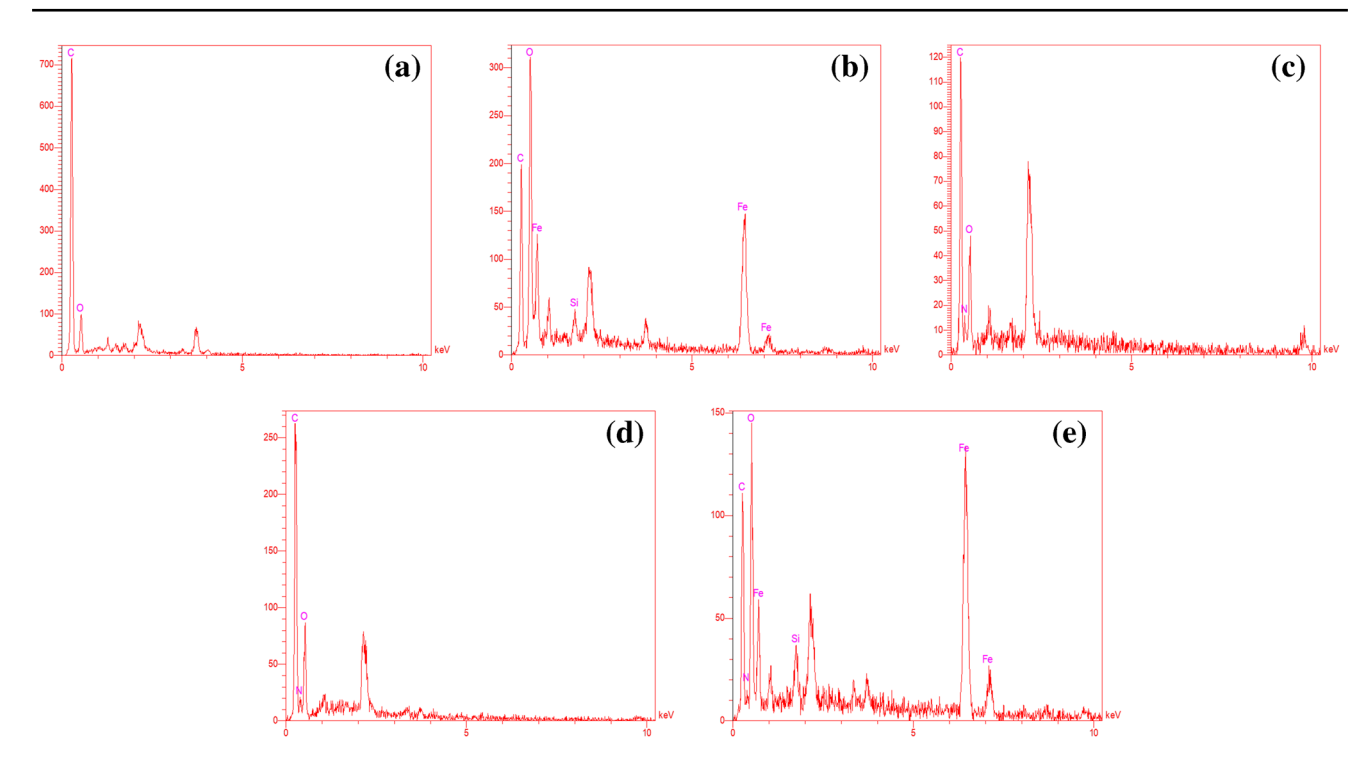
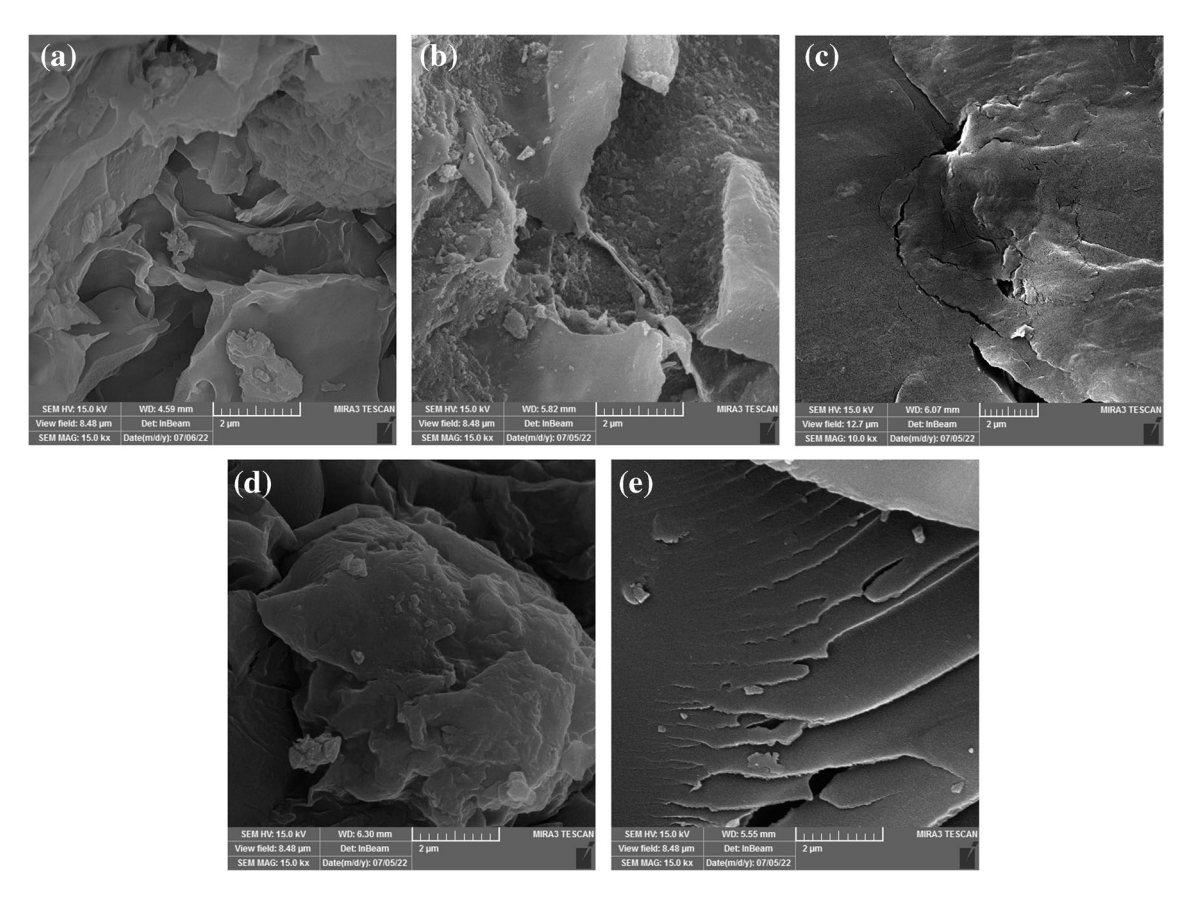


Fig. 3 EDS spectra of a) BC, b) MTWBC, c) HG, d) HG/BC, and e) HG/MTWBC



 $\textbf{Fig. 4} \ \ \text{FESEM images of } \textbf{a}) \ BC, \ \textbf{b}) \ \text{MTWBC}, \ \textbf{c}) \ \text{HG}, \ \textbf{d}) \ \text{HG/BC}, \ \text{and} \ \textbf{e}) \ \text{HG/MTWBC} \ \text{after MB adsorption with magnification of 2} \ \mu\text{m}$



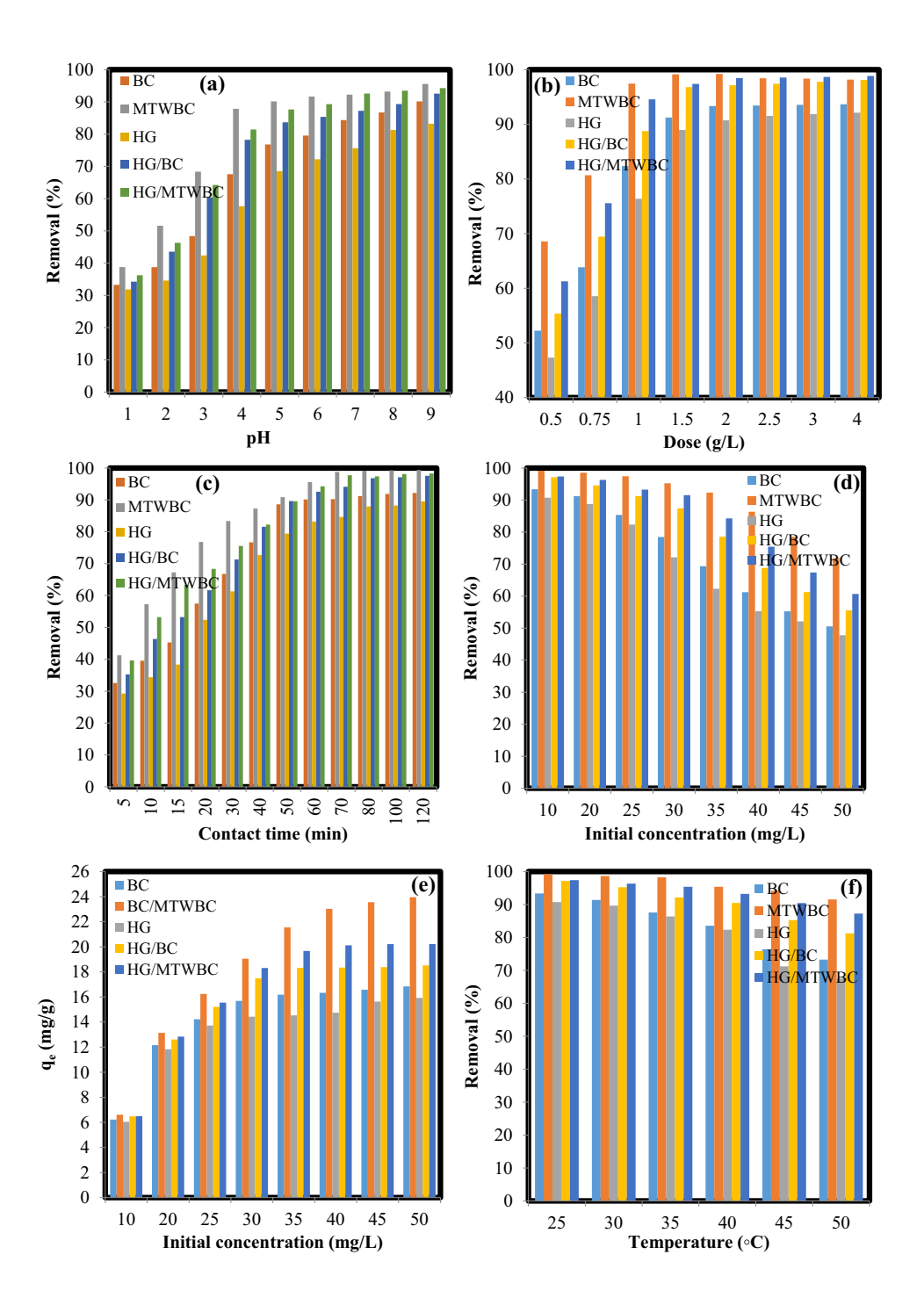
As depicted in Fig. 5b, the removal performance of MTWBC and HG/MTWBC was enhanced from 68.56 and 61.28% to 99.16 and 97.39%, respectively, as the adsorbent dose was elevated from 0.5 to 1.5 g/L. Also, the removal performance of BC, HG, and HG/BC hydrogel was increased from 52.24, 47.23, and 55.26% to 93.35, 90.74, and 97.15%, respectively, when the adsorbent dose was increased from 1.5 to 4 g/L. The surface area and the number of binding sites were enhanced by incrementing the adsorbent dose, increasing removal performance. The

removal performance of adsorbents remains constant with a further increase of adsorbents' dose from the optimum value. These can be related to the aggregation of adsorbents' particles, which restricts the achievement of MB molecules in sorption sites.

3.2.3 Impact of contact time

To benefit more from the removal ability of adsorbents, it is essential to assess the contact time parameter because

Fig. 5 Effect of a) pH, b) adsorbent dose, c) contact time, d) initial concentration e) effect of initial concentration on equilibrium adsorption capacity (q_e(mg/g)), and f) temperature on removal performance and of BC, MTWBC, HG, HG/BC, and HG/MTWBC





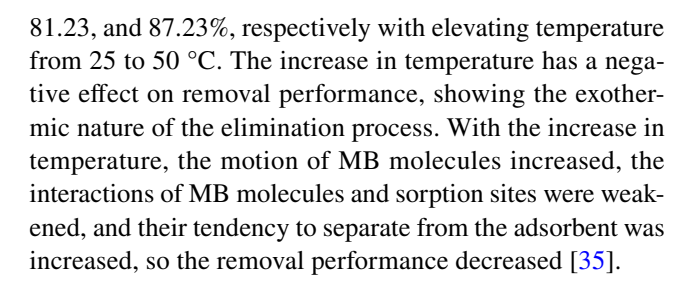
the adsorbents must have enough time to access and interact with dye molecules. From an economic perspective, adsorbents must be able to remove pollutants from wastewater quickly. This study investigated the effect of contact time on the removal performance of BC, MTWBC, HG, HG/BC, and HG/MTWBC adsorbents in the 50–120 min range. As depicted in Fig. 5c, the rate of MB removal by synthesized adsorbents was enhanced sharply in the first 30 min, and then it slowed down until reaching an equilibrium state. In the first minutes of the adsorption process, most adsorption sites are vacant to interact with more dye molecules through various mechanisms such as hydrogen bonding, electrostatic interaction, and π-π interactions. By further increase of contact time, the adsorption sites of adsorbents got involved with MB molecules, so the rate of the removal process was decreased, and removal performance reached an equilibrium state [34]. The equilibrium contact time for BC, MTWBC, HG, HG/BC, and HG/ MTWBC adsorbents was obtained in 70 min.

3.2.4 Impact of dye initial concentration

The effect of MB initial concentration on the removal performance of BC, MTWBC, HG, HG/BC, and HG/ MTWBC adsorbents was studied in 10-50 mg/L. According to Fig. 5d, the removal performance of BC, MTWBC, HG, HG/BC, and HG/MTWBC adsorbents decreased from 93.35, 99.16, 90.74, 97.15, 97.39% to 50.54, 71.86, 47.78, 55.56, and 60.67%, respectively with the increase of dye initial concentration from 10 to 50 mg/L. The saturation of sorption sites with MB molecules is the main cause of the decrement in removal performance. According to Fig. 5e, the equilibrium adsorption capacity of BC, MTWBC, HG, HG/BC, and HG/MTWBC adsorbents was enhanced from 6.22, 6.61, 6.05, 6.48, and 6.49 mg/g to 16.85, 23.95, 15.93, 18.52, and 20.22 mg/g, respectively with increase of dye initial concentration from 10 to 50 mg/L. The mass driving force is increased by incrementing initial concentration, enhancing equilibrium adsorption capacity. The equilibrium adsorption capacity of BC, MTWBC, HG, HG/BC, and HG/MTWBC adsorbents was found to be 16.18, 23.02, 14.43, 18.33, and 20.12 mg/g, respectively. The optimum value of the dye's initial concentration was 10 mg/L based on removal performance.

3.2.5 Impact of temperature

The effect of initial concentration on the removal performance of BC, MTWBC, HG, HG/BC, and HG/MTWBC adsorbents was studied in the 25–50 °C range. According to Fig. 5f, the removal performance of BC, MTWBC, HG, HG/BC, and HG/MTWBC adsorbents was decreased from 93.35, 99.16, 90.74, 97.15, 97.39% to 73.25, 91.54, 67.56,



3.3 Kinetic study

The kinetic study was performed by pseudo-first-order (PSF), pseudo-second-order (PSO), and intra-particle diffusion (IPD) models represented with Eqs. (3–5):

$$Ln(q_e - q_t) = Ln(q_e) - k_1 t$$
(3)

$$\frac{t}{q_{t}} = \frac{t}{q_{e}} + \frac{1}{k_{2}q_{e}^{2}} \tag{4}$$

$$q_{t} = k_{i,d} t^{0.5} + I_{i} \tag{5}$$

The fitting findings were depicted in Fig. 6a-c, and regression coefficients were tabulated in Table 2. The findings showed that the R^2 value for the PSO model is higher and closer to one, so it is the best model for fitting kinetic data. Also, the amount of $q_{\rm e,cal}$ is closer to $q_{\rm e}$, showing this model's high accuracy in fitting and predicting kinetic data. The IPD model was used to study the diffusion of MB molecules to synthesized adsorbents. The results showed that diffusion of MB molecules happens in two stages. In the first stage, MB molecules diffuse from a thin layer called the boundary layer diffusion stage. In the second stage, MB molecules diffuse through the pores of adsorbents and interact with sorption sites. The rate of the first stage is higher than the second stage, so the second stage mainly controls MB adsorption.

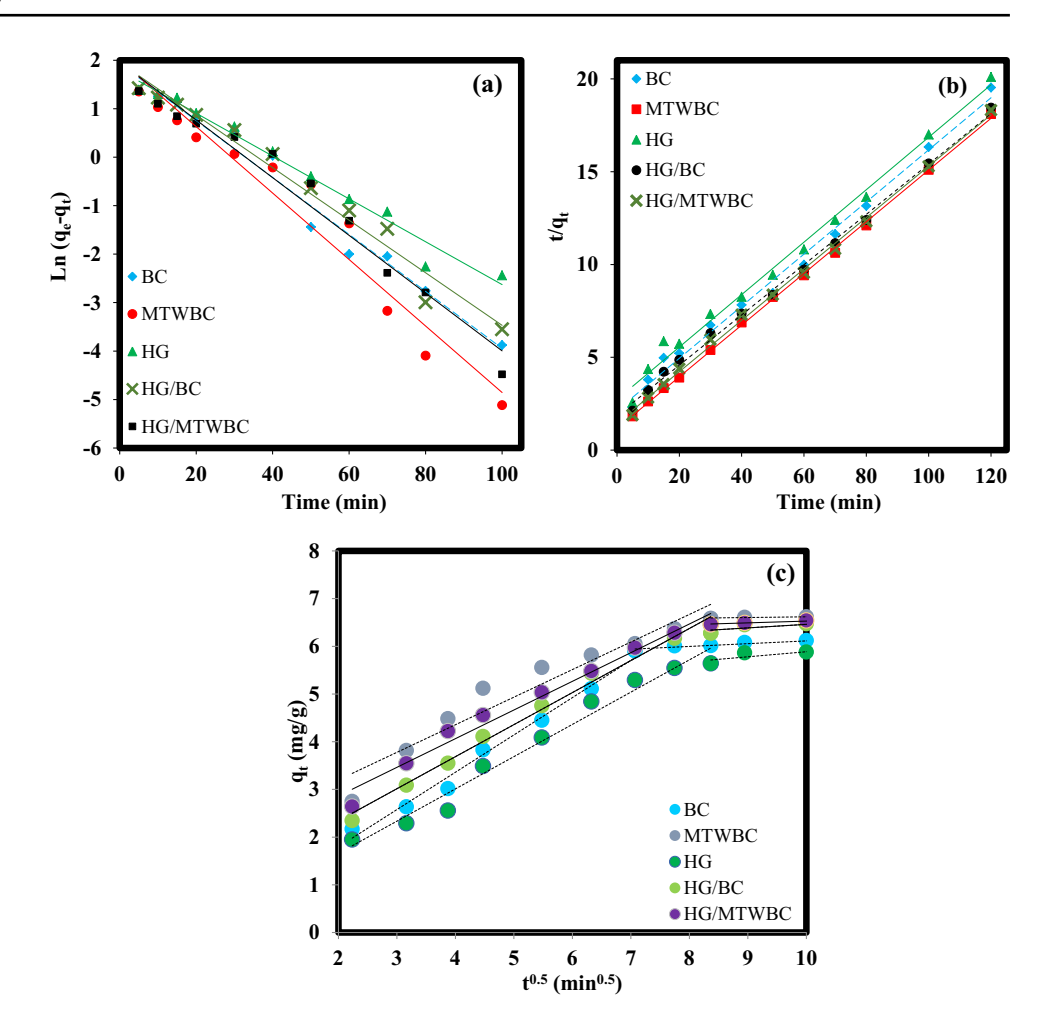
 $q_e\colon$ calculated equilibrium adsorption capacity, k_1 (min $^{-1}$): rate constant of quasi-first-order, k_2 (g/mg/min): rate constant of quasi-second-order, $K_{i,d}\colon$ intra-particle diffusion rate constant, and $I_i\colon$ a constant related to the boundary layer.

3.4 Isotherm study

The isotherm study provides valuable information about the interactions between adsorbents and adsorbate. Langmuir (Eq. 6), Freundlich (Eq. 7), Temkin (Eq. 8), and Dubin-Radeshkewinch (D-R, Eq. 9) models are widely applied to fitting equilibrium data:



Fig. 6 Linear regression of kinetic models a) PFO, b) PSO, and c) IPD model



 $\begin{tabular}{ll} \textbf{Table 2} & Kinetic parameters for BC, MTWBC, HG, HG/BC, and HG/MTWBC \end{tabular} \label{eq:matches}$

Kinetic models	Adsorbe	ent			
	BC	MTWBC	HG	HG/BC	HG/MTWBC
		Pseudo-fii	rst-order	,	
$q_{e,cal}$ (mg/g)	6.89	7.404	6	7.046	7.099
$k_1(min^{-1})$	0.056	0.068	0.044	0.068	0.062
\mathbb{R}^2	0.976	0.949	0.978	0.972	0.969
		Pseudo-se	cond-or	der	
$q_{e,cal}$ (mg/g)	7.127	7.38	7.077	7.183	7.23
k ₂ (g/mg/min)	0.009	0.0165	0.007	0.009	0.013
$q_{e,exp}$ (mg/g)	6.145	6.627	5.969	6.504	6.554
\mathbb{R}^2	0.992	0.992	0.991	0.996	0.998
		Intra-par	ticle diff	usion	
$k_{i,1}$	0.7824	0.5781	0.6762	0.6717	0.601
I_1	0.2307	2.0439	0.3066	0.999	1.6588
\mathbb{R}^2	0.987	0.932	0.9751	0.985	0.978
$k_{i,2}$	0.058	0.0148	0.1057	0.074	0.0364
I_2	5.535	6.47	4.8286	5.7191	6.1643
\mathbb{R}^2	0.908	0.83	0.7697	0.682	0.9386

$$\frac{C_{e}}{q_{e}} = \frac{C_{e}}{q_{m}} + \frac{1}{K_{L}q_{m}}R_{L} = \frac{1}{1 + K_{L}C_{i}}$$
 (6)

$$\underline{C} \qquad Ln(q_e) = Ln(K_F) + \frac{1}{n} Ln(C_e)$$
(7)

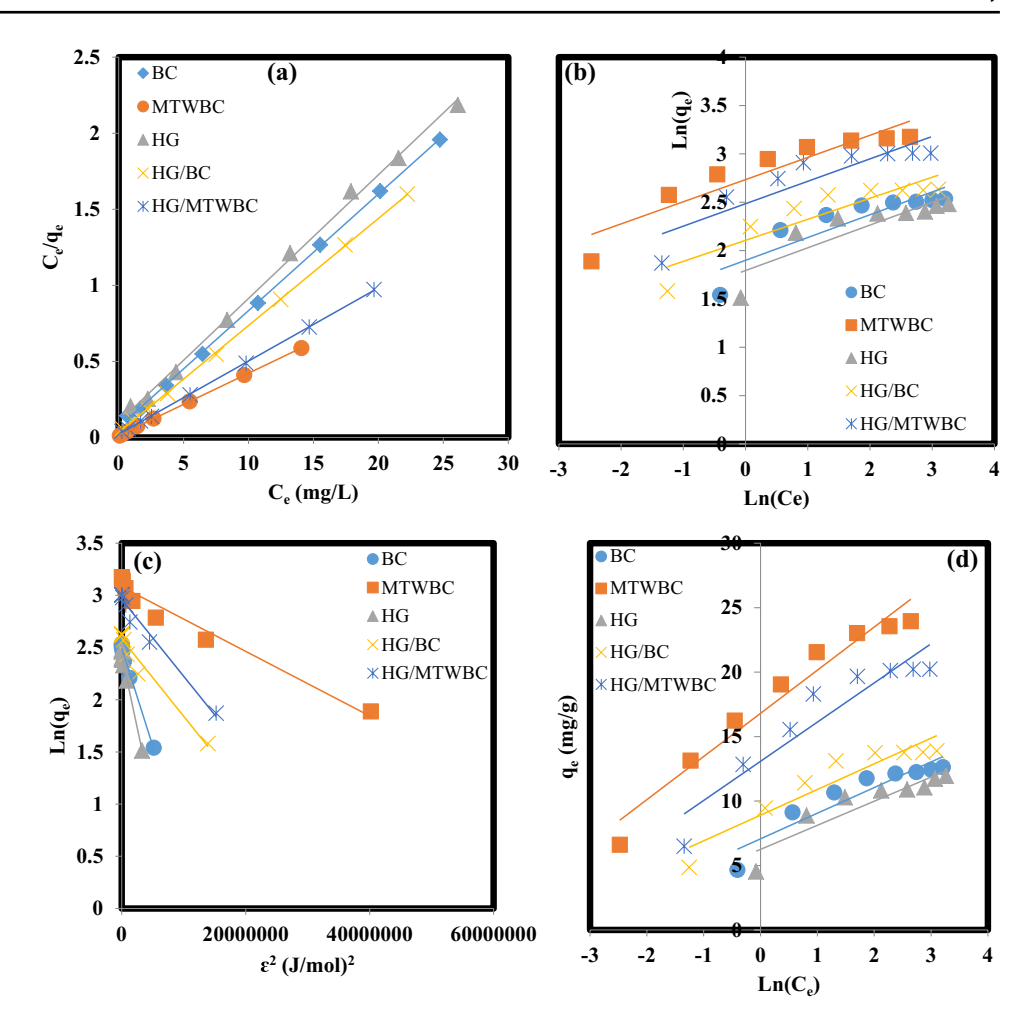
$$q_e = BLn(K_T) + BLn(C_e), B = \frac{RT}{h}$$
(8)

$$Ln(q_e) = Ln(q_s) - \beta \varepsilon^2 \ \varepsilon = R \ T \ Ln\left(1 + \frac{1}{C_e}\right) E_a = \frac{1}{\sqrt{2}\beta}$$
(9)

The results of equilibrium data fitting were demonstrated in Fig. 7a-d, and coefficients of isotherm models were tabulated in Table 3. Based on the fitting findings, the Langmuir model is the most appropriate for describing the interaction of MB molecules and synthesized adsorbents. It can be concluded from the governing of the Langmuir model that a monolayer of MB molecules covers the surface of adsorbents without interactions



Fig. 7 Curves of linear regression of isotherm models a)
Langmuir, b) Freundlich, c)
D-R, and d) Temkin



between them, and the surface of adsorbents is homogenous [36]. The maximum adsorption capacity (q_{max}) of BC, MTWBC, HG, HG/BC, and HG/MTWBC adsorbents was computed to be 13.054, 24.39, 12.3, 14.2, and 20.79 mg/g, respectively. The dimensionless separation factor (R_L) value for all synthesized adsorbents is 0–1, showing the desirability of MB molecules in interacting with adsorbents [37]. The performance of synthesized adsorbents in removing MB molecules was consistent with other previous studies, and the results are presented in Table 4. It can be inferred that the synthesized adsorbents can potentially eliminate MB molecules from wastewater.

3.5 Thermodynamic study

Thermodynamic feasibility and thermal effects of MB sorption were studied by computing thermodynamic parameters such as change in free Gibbs energy (ΔG°), change in free enthalpy (ΔH° , and change in free entropy (ΔS°). Van't Hoff formula (Eq. 12) was used to calculate ΔH° and ΔS° , obtained from the slope and intercept of

this equation plot, respectively. The plot of the Van't Hoff formula and calculated thermodynamic parameters were presented in Fig. 8 and Table 5, respectively.

$$K_D = \frac{q_e}{C_e} \tag{10}$$

$$Ln(K_D) = -\frac{\triangle H^{\circ}}{RT} + \frac{\triangle S^{\circ}}{R}$$
(11)

$$\triangle G^{\circ} = -R \ T \ Ln(K_D) \tag{12}$$

The change in free enthalpy for BC, MTWBC, HG, HG/BC, and HG/MTWBC adsorbents were computed to be -55.224, -80.246, -53.899, -65.339, -54.73 kJ/mol, respectively. Hence, MB adsorption to synthesized adsorbents is exothermic. The calculated (ΔS°) for BC, MTWBC, HG, HG/BC, and HG/MTWBC adsorbents were -19.605, -27.548, -19.308, -22.911, and -18.427 J/mol.K, respectively. The negative values of change in free entropy demonstrate that the randomness of MB



 $\begin{tabular}{ll} \textbf{Table 3} & Isotherm & parameters & for BC, MTWBC, HG, HG/BC, and HG/MTWBC \\ \end{tabular}$

Isotherm			Adsorbe	nt	
models	BC	MTWBC	HG	HG/BC	HG/MTWBC
	Langm	uir			
q _{max} (mg/g)	13.054	24.39	12.3	14.2	20.79
$K_L(L/mg)$	1.136	3.2	0.8	2.22	2.24
\mathbb{R}^2	0.997	0.999	0.9976	0.9998	0.9998
	Freund	lich			
n	4.233	4.45	4.255	4.593	4.31
$K_F (mg/g.(L/mg)^{1/n})$	6.67	15.74	7.316	8.2	11.97
\mathbb{R}^2	0.791	0.818	0.766	0.809	0.796
	D-R				
E (kJ/mol)	0.017	0.032	0.019	0.021	0.021
$q_{m} (mg/g)$	12.11	21.8	11.311	13.23	19.33
\mathbb{R}^2	0.98	0.8112	0.96	0.96	0.973
	Temkin	1			
b _T (KJ/mol)	1.245	0.87	1.327	1.24	0.816
$K_T(1/g)$	35.03	218.54	28.56	80.15	74.52
\mathbb{R}^2	0.87	0.903	0.854	0.87	0.88

 q_m (mg/g): maximum adsorption capacity, K_L (L/mg): Langmuir adsorption constant, K_F and n: Freundlich model constants, b_T (J/mol) and K_T (1/g): Temkin constants, R: universal constant of gases, T(K): Absolute temperature, ϵ : Polany coefficient and β (mol/g)²: activity coefficient.

molecules was decreased by rising temperature. As summarized in Table 5, the negative values of change in free Gibbs energy for MB sorption by BC, MTWBC, HG, HG/BC, and HG/MTWBC adsorbents showed spontaneous decontamination [42].

Table 4 Comparison of MB adsorption by pervious literatures with the present study

Adsorbent	Initial concentra- tion (mg/L)	Qm (mg/g)	Ref
N-Isopropylacrylamide	10–50	8.5	[38]
N-Isopropylacrylamide/Itaconic acid	10-50	17.52	[38]
Carboxylmethyl cellulose coated Fe ₃ O ₄ @ SiO ₂ magnetic nanoparticles	100	17.5	[39]
Carboxymethyl cellulose/k-carrageenan/activated montmorillonite	10–500	10.75	[40]
Ficcus Palmata leaves	5–25	6.8	[41]
BC	10-50	13.054	This work
MTWBC	10-50	24.39	This work
HG	10-50	12.3	This work
HG/BC	10-50	14.2	This work
HG/MTWBC	10-50	20.79	This work

3.6 Mechanism of MB adsorption

Adsorption of MB molecules to synthesized adsorbents happens with various mechanisms, which depend on the pH of water media, textural properties of adsorbents, and physicochemical properties of adsorbents and adsorbate. In the primary medium, synthesized adsorbents have a negative surface charge due to the dissociation of BC and CMC carboxyl groups; hence, they can interact with cationic MB molecules via electrostatic interactions. Hydrogen bonding is another effective mechanism in the sorption of MB molecules, which is formed between hydroxyl and amine groups of adsorbents and -NH of MB molecules. The amine groups of hydrogel and nanocomposite hydrogels are related to the presence of poly(acrylamide). Another recommended adsorption mechanism is π - π interaction between the π electrons of BC and benzene rings of MB molecules [43]. According to the BET and SEM analysis findings, the synthesized adsorbents have a porous structure, so pore filling is another recommended mechanism for MB sorption. FTIR analysis was performed to investigate and confirm mechanisms of MB sorption, and the results were demonstrated in the following Fig. 9a-e. In the FTIR spectra of BC and MTWBC after MB sorption, the intensity of the -OH peak located around 3438 cm⁻¹ was decreased due to forming a hydrogen bond with -NH of MB. Also, the intensity of -C = O and -C-O bands located around 1732 and 1276 cm⁻¹, respectively, was changed due to the formation of electrostatic interaction between carboxyl groups of BC and MTWBC and -NH²⁺ moieties of MB.

In the FTIR spectra of HG, HG/BC, and HG/MTWBC after MB sorption, hydrogen bonding is formed between



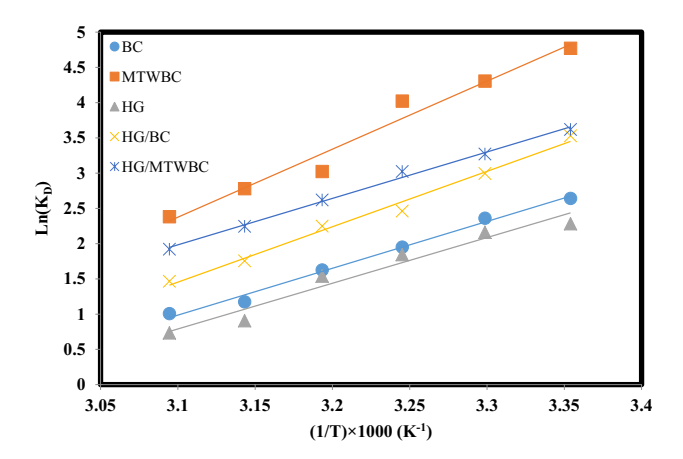


Fig. 8 Linear relation between Ln (K_D) and 1/T

–NH of MB and –OH and –NH of adsorbents, which is confirmed by the intensity change of overlapped peak of –NH and –OH groups located around 3437 cm⁻¹. Also, the intensity change of –C = O (~1730 cm⁻¹) and –C-O (~1280 cm⁻¹) confirms the electrostatic interaction between cationic MB and adsorbents. The scheme of MB sorption by HG/MTWBC is represented in Fig. 10.

4 Conclusion

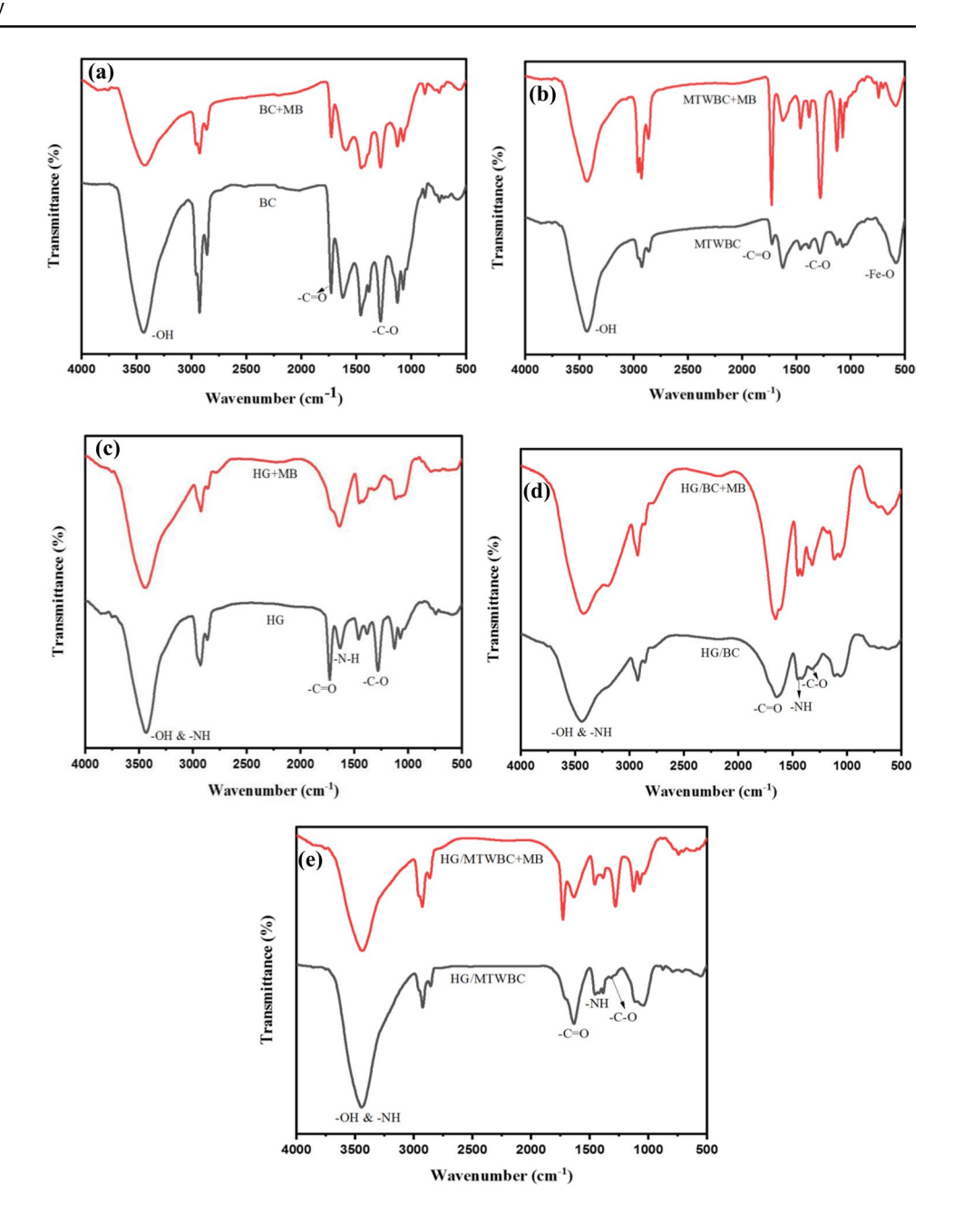
The present study synthesized HG/MTWBC nanocomposite hydrogel as a novel magnetic adsorbent to eliminate MB from water media. The pyrolysis method synthesized BC from tea waste as a natural and abundant source. BC was doped successfully with Fe₃O₄ nanoparticles to magnetize the adsorbent and enhance its removal performance. An optimum value of MTWBC (10 wt.%) was incorporated into HG, and the results showed an enhancement in removal performance and magnetic separation of the adsorbent. The SEM and BET results showed that HG/MTWBC nanocomposite hydrogel has a fine porous structure with significant surface areas for the adsorption of MB. Assessment of FTIR results showed the presence of -OH and -COOH groups in the structure of the adsorbent and their participation in the MB removal process through hydrogen bonding and electrostatic interaction. According to experimental results, the maximum removal performance of 83.22 (for HG), 92.57 (for HG/BC), and 94.27% (for HG/MTWBC) was obtained at optimum conditions of pH 8, dose 1.5 g/L, initial concentration 10 mg/L, contact time 70 min, and temperature 25 °C. Analyzing kinetic data showed that most parts of MB molecules adsorb to adsorbents by chemisorption mechanism due to the government of the PSO model. The Langmuir model can be used to fit equilibrium data with high accuracy, and the monolayer adsorption capacities of HG, HG/BC, and HG/

10	ΔG° (kJ/mol)							ΔH° (KJ/mol)	ΔS° (J/mol K)
	T(°C)	25	30	35	40	45	50		
BC		-6.543	-5.945	-4.993	-4.215	-3.093	-2.704	-55.224	-19.605
MTWBC		-11.818	-10.847	-10.299	-7.864	-6.001	-6.393	-80.246	-27.548
HG		-5.653	-5.443	-4.711	4-	-2.395	-1.968	-53.889	-19.308
HG/BC		-8.74	-7.539	-6.301	-5.849	-4.639	-3.934	-65.339	-22.911
HG/MTWBC		-8.966	-8.237	-7.738	-6.815	-5.932	-5.158	-54.73	-18.427

Table 5 Thermodynamic parameters of MB decontamination process



Fig. 9 FTIR spectra of a) BC, b) MTWBC, c) HG, d) HG/BC, and e) HG/MTWBC before and after MB adsorption



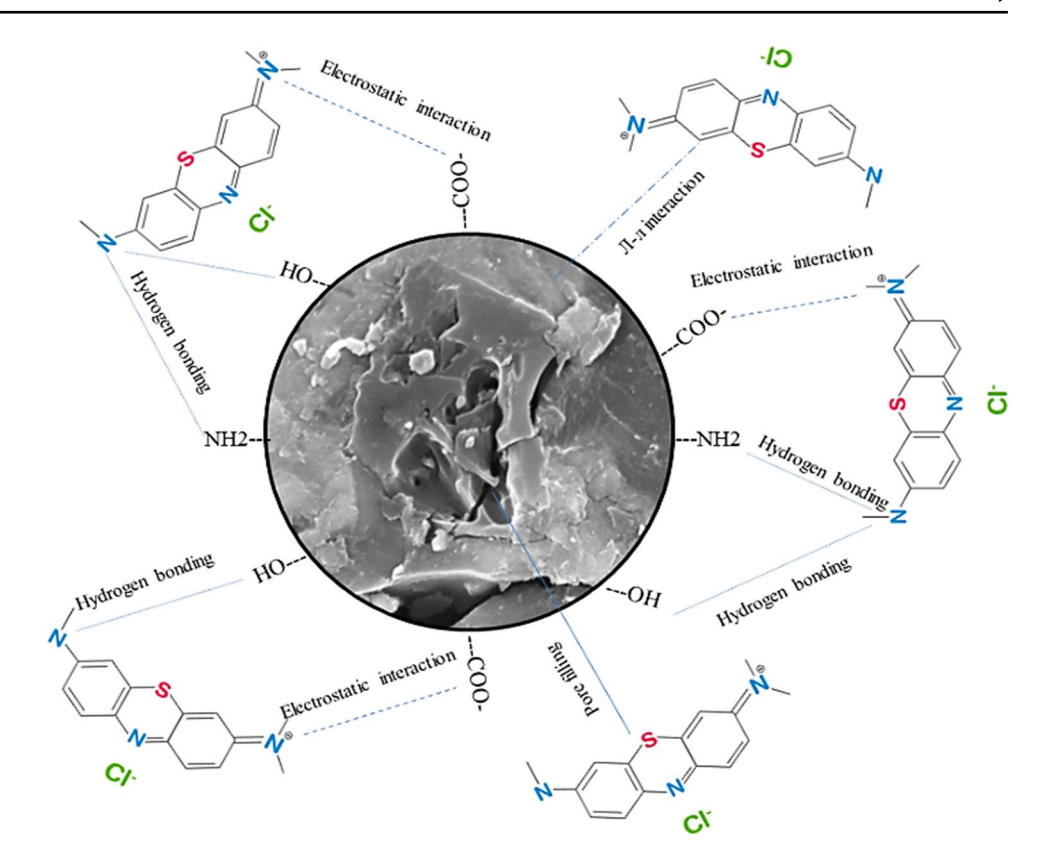
MTWBC nanocomposite hydrogels were found to be 12.3, 14.2, and 20.79 mg/g, respectively. The thermodynamic study showed that MB sorption to synthesized adsorbents is favorable, spontaneous, and exothermic. Finally, it can be concluded that HG/MTWBC magnetic nanocomposite hydrogel can be applied as a promising adsorbent to eliminate MB from water media.

5 Funding sources

This research was conducted without commercial or financial relationships that could be construed as a potential conflict of interest. The authors, therefore, declare no conflict of interest.



Fig. 10 Scheme of MB sorption by HG/MTWB



Authors' contribution Seyed Jamaleddin Peighambardoust designed the study, interpreted the results, and revised the manuscript critically for important intellectual content; Mina Mollazadeh Azari performed the samples' synthesis and collected test data; Parisa Mohammadzadeh Pakdel drafted the manuscript, and Rauf Foroutan advising on Conceptualization. All authors approve the final version of the manuscript and agree to be accountable for all aspects of the work.

Declarations

Conflict of interest All authors approve the final version of the manuscript and agree to be accountable for all aspects of the work.

References

- Oladoye PO, Ajiboye TO, Omotola EO, Oyewola OJ (2022) Methylene blue dye: Toxicity and potential elimination technology from wastewater. Results Eng 16:100678
- Dehingia B, Lahkar R, Kalita H (2024) Efficient removal of both cationic and anionic dyes from water using a single rGO/PSS nanocomposite membrane with superior permeability and high aqueous stability. J Environ Chem Eng 12:112393
- Khasim S, Dastager SG, Alahmdi MI, Hamdalla TA, Ulla MF, Panneerselvam C et al (2024) Green synthesis of multifunctional Cu/MnO@Biochar 3D structure as a high-performance anode material in Li-ion batteries and oxidative removal of Cango-red dye. Case Stud Chem Environ Eng 9:100561
- Cimen A, Bilgic A, Bayrak M (2024) Fabrication and characterization of new Fe₃O₄@SiO₂@TiO₂-CPTS-HBAP (FST-CH) nanoparticles for photocatalytic degradation and adsorption removal of rhodamine B dye in the aquatic environment. Heliyon. 10:e29355

- Ihaddaden S, Aberkane D, Boukerroui A, Robert D (2022) Removal of methylene blue (basic dye) by coagulation-flocculation with biomaterials (bentonite and Opuntia ficus indica). J Water Process Eng 49:102952
- Benhalima T, Sadi A, Dairi N, Ferfera-Harrar H (2024) Multifunctional carboxymethyl cellulose-dextran sulfate/AgNPs@zeolite hydrogel beads for basic red 46 and methylene blue dyes removal and water disinfection control. Sep Purif Technol 342:127001
- Algethami JS, Jugade R, Billah El Kaim R, Bahsis L, Achak M, Majdoubi H et al (2024) Chitin extraction from crab shells and synthesis of chitin @metakaolin composite for efficient amputation of Cr (VI) ions. Environ Res 252:119065
- Hui Y, Liu R, Lan J, Tiantian S, Xu A (2024) Recyclable chitosan adsorbent: Facile functionalization strategy, excellent removal capacity of dyes and adsorption mechanism. Chemosphere 359:142291
- Zhu H, Chen S, Duan H, He J, Luo Y (2023) Removal of anionic and cationic dyes using porous chitosan/carboxymethyl cellulose-PEG hydrogels: Optimization, adsorption kinetics, isotherm and thermodynamics studies. Int J Biol Macromol 231:123213
- Asadi S, Eris S, Azizian S (2018) Alginate-based hydrogel beads as a biocompatible and efficient adsorbent for dye removal from aqueous solutions. ACS Omega 3:15140–15148
- Ren J, Wang X, Zhao L, Li M, Yang W (2022) Double network gelatin/chitosan hydrogel effective removal of dyes from aqueous solutions. J Polym Environ 30:2007–2021
- Alqarni LS, Algethami JS, El KaimBillah R, Alorabi AQ, Alnaam YA, Algethami FK et al (2024) A novel chitosan-alginate@Fe/Mn mixed oxide nanocomposite for highly efficient removal of Cr (VI) from wastewater: Experiment and adsorption mechanism. Int J Biol Macromol 263:129989
- El KaimBillah R, Zaghloul A, L. bahsis, N. A. Oladoja, Z. azoubi, A. taoufyk, et al (2024) Multifunctional biocomposites



- based on cross-linked Shrimp waste-derived chitosan modified Zn²⁺@Calcium apatite for the removal of methyl orange and antibacterial activity. Mater Today Sustain 25:100660
- Hossieni-Aghdam SJ, Foroughi-Nia B, Zare-Akbari Z, Mojarad-Jabali S, H. motasadizadeh, and H. Farhadnejad, (2018) Facile fabrication and characterization of a novel oral pH-sensitive drug delivery system based on CMC hydrogel and HNT-AT nanohybrid. Int J Biol Macromol 107:2436–2449
- Cen C, Wang F, Wang Y, Li H, Fu L, Li Y et al (2023) Design and characterization of an antibacterial film composited by hydroxyethyl cellulose (HEC), carboxymethyl chitosan (CMCS), and nano ZnO for food packaging. Int J Biol Macromol 231:123203
- Liang J, Yan Y, Chen L, Wu J, Li Y, Zhao Z et al (2023) Synthesis of carboxymethyl cellulose-g-poly (acrylic acid-co-acrylamide)/ polyvinyl alcohol sponge as a fast absorbent composite and its application in coral sand soil. Int J Biol Macromol 242:124965
- MohammadzadehPakdel P, Peighambardoust SJ, Foroutan R, Arsalani N, Aghdasinia H (2022) Decontamination of Fuchsin dye by carboxymethyl cellulose-graft-poly(acrylic acid-co-itaconic acid)/carbon black nanocomposite hydrogel. Int J Biol Macromol 222:2083–2097
- Nagarpita MV, Roy P, Shruthi SB, Sailaja RRN (2017) Synthesis and swelling characteristics of chitosan and CMC grafted sodium acrylate-co-acrylamide using modified nanoclay and examining its efficacy for removal of dyes. Int J Biol Macromol 102:1226–1240
- Yang L, Bao L, Dong T, Xie H, Wang X, Wang H et al (2023) Adsorption properties of cellulose/guar gum/biochar composite hydrogel for Cu²⁺, Co²⁺ and methylene blue. Int J Biol Macromol 242:125021
- Elshahawy MF, Ahmed NA, Gad YH, Ali AEH (2024) Efficient photocatalytic remediation of lerui acid brilliant blue dye using radiation- prepared carboxymethyl cellulose/acrylic acid hydrogel supported by ZnO@Ag. Int J Biol Macromol 262:129946
- MohammadzadehPakdel P, Peighambardoust SJ, Arsalani N, Aghdasinia H (2022) Safranin-O cationic dye removal from wastewater using carboxymethyl cellulose-grafted-poly(acrylic acid-coitaconic acid) nanocomposite hydrogel. Environ Res 212:113201
- Laddha H, Jadhav NB, Agarwal M, Gupta R (2023) Enumeration
 of research journey of MOF@hydrogel composite beads as potential adsorbents for adsorptive elimination of toxic contaminants. J
 Environ Chem Eng 11:110642
- Wang X, Guo Z, Hu Z, Zhang J (2020) Recent advances in biochar application for water and wastewater treatment: a review. PeerJ 8:e9164
- Khan TA, Saud AS, Jamari SS, Rahim MHA, Park J-W, Kim H-J (2019) Hydrothermal carbonization of lignocellulosic biomass for carbon rich material preparation: A review. Biomass Bioenergy 130:105384
- Kulal P, Badalamoole V (2021) Evaluation of gum ghattig-poly(itaconic acid) magnetite nanocomposite as an adsorbent material for water purification. Int J Biol Macromol 193:2232-2242
- Tahmasebpour R, Peighambardoust SJ (2024) Decontamination of tetracycline from aqueous solution using activated carbon/Fe₃O₄/ ZIF-8 nanocomposite adsorbent. Sep Purif Technol 343:127188
- Algethami JS, Alhamami MAM, Alqadami AA, Melhi S, Seliem AF (2024) Magnetic hydrochar grafted-chitosan for enhanced efficient adsorption of malachite green dye from aqueous solutions: Modeling, adsorption behavior, and mechanism analysis. Int J Biol Macromol 254:127767
- SakhaeiNiroumand J, Peighambardoust SJ, Mohammadi R (2024)
 Tetracycline decontamination from aqueous media using nanocomposite adsorbent based on starch-containing magnetic montmorillonite modified by ZIF-67. Int J Biol Macromol 259:129263
- Foroutan R, Peighambardoust SJ, Mohammadi R, Ramavandi B, Boffito DC (2021) One-pot transesterification of non-edible Moringa oleifera oil over a MgO/K₂CO₃/HAp catalyst derived from poultry skeletal waste. Environ Technol Innov 21:101250

- Boukhalfa N, Boutahala M, Djebri N, Idris A (2019) Kinetics, thermodynamics, equilibrium isotherms, and reusability studies of cationic dye adsorption by magnetic alginate/oxidized multiwalled carbon nanotubes composites. Int J Biol Macromol 123:539–548
- Abbas RF, Hassan MJM, Rheima AM (2024) Adsorption of Fast Green dye onto Fe₃O₄ MNPs and GO/Fe₃O₄ MNPs Synthesized by Photo-Irradiation method: Isotherms, Thermodynamics, Kinetics, and Reuse Studies. Sustain Chem Environ 6:100104
- 32. Zhang Y, Shao D, Yan J, Jia X, Li Y, Yu P et al (2016) The pore size distribution and its relationship with shale gas capacity in organic-rich mudstone of Wufeng-Longmaxi Formations, Sichuan Basin, China. J Nat Gas Geosci 1(3):213–20
- Hosseini H, Zirakjou A, McClements DJ, Goodarzi V, Chen WH (2022) Removal of methylene blue from wastewater using ternary nanocomposite aerogel systems: Carboxymethyl cellulose grafted by polyacrylic acid and decorated with graphene oxide. J Hazard Mater 421:126752
- Alizadeh M, Peighambardoust SJ, Foroutan R (2024) Efficacious adsorption of divalent nickel ions over sodium alginate-gpoly(acrylamide)/hydrolyzed Luffa Cylindrica-CoFe₂O₄ bionanocomposite hydrogel. Int J Biol Macromol 254:127750
- 35 Foroutan R, Peighambardoust SJ, Hemmati S, Khatooni H, Rama-vandi B (2021) Preparation of clinoptilolite/starch/CoFe₂O₄ magnetic nanocomposite powder and its elimination properties for cationic dyes from water and wastewater. Int J Biol Macromol 189:432–442
- Mittal H, Al Alili A, Morajkar PP, Alhassan SM (2021) GO crosslinked hydrogel nanocomposites of chitosan/carboxymethyl cellulose A versatile adsorbent for the treatment of dyes contaminated wastewater. Int J Biol Macromol 167:1248–1261
- 37. Parlayici Ş, Aras A (2024) Synthesis of a novel green biopolymer-based composites beads for removal of methylene blue from aquatic medium: isotherm, thermodynamic and kinetic investigation. Polym Bull 81:6603–6640
- Taşdelen B, Çifçi Dİ, Meriç S (2017) Preparation of N-isopropylacrylamide/itaconic acid/Pumice highly swollen composite hydrogels to explore their removal capacity of methylene blue. Colloids Surf, A 519:245–253
- Zirak M, Abdollahiyan A, Eftekhari-Sis B, Saraei M (2018) Carboxymethyl cellulose coated Fe₃O₄@SiO₂ core–shell magnetic nanoparticles for methylene blue removal: equilibrium, kinetic, and thermodynamic studies. Cellulose 25:503–515
- Liu C, Omer A, Ouyang XK (2018) Adsorptive removal of cationic methylene blue dye using carboxymethyl cellulose/k-carrageenan/activated montmorillonite composite beads: Isotherm and kinetic studies. Int J Biol Macromol 106:823–833
- 41. Fiaz R, Hafeez M, Mahmood R (2019) Ficcus palmata leaves as a low-cost biosorbent for methylene blue: Thermodynamic and kinetic studies. Water Environ Res 91:689–699
- Al-Asadi ST, Al-Qaim FF, Al-Saedi HFS, Deyab IF, Kamyab H, Chelliapan S (2023) Adsorption of methylene blue dye from aqueous solution using low-cost adsorbent: kinetic, isotherm adsorption, and thermodynamic studies. Environ Monit Assess 195:676
- 43. Hegazy S, Abdelwahab NA, Ramadan AM, Mohamed SK (2024) Magnetic Fe₃O₄-grafted cellulose/graphene oxide nanocomposite for methylene blue removal from aqueous solutions: Synthesis and characterization. Next Mater 3:100064

Publisher's Note Springer Nature remains neutral with regard to jurisdictional claims in published maps and institutional affiliations.

Springer Nature or its licensor (e.g. a society or other partner) holds exclusive rights to this article under a publishing agreement with the author(s) or other rightsholder(s); author self-archiving of the accepted manuscript version of this article is solely governed by the terms of such publishing agreement and applicable law.

